Eur Biophys J (2000) 29: 487–498
DOI 10.1007/s002490000096

ARTICLE

**E. Błachut-Okrasińska · E. Bojarska · A. Niedźwiecka
L. Chlebicka · E. Darżynkiewicz · R. Stolarski
J. Stępiński · J. M. Antosiewicz**

Stopped-flow and Brownian dynamics studies of electrostatic effects in the kinetics of binding of 7-methyl-GpppG to the protein eIF4E

Received: 2 May 2000 / Revised version: 17 July 2000 / Accepted: 17 July 2000 / Published online: 15 September 2000

Abstract The kinetics of binding 7-methyl-GpppG, an analogue of the 5′-mRNA cap, to the cap-binding protein eIF4E, at 20 °C, in 50 mM Hepes-KOH buffer, pH 7.2, and 50, 150 and 350 mM KCl, was measured using a stopped-flow spectrofluorometer, and was simulated by means of a Brownian dynamics method. For most of the stopped-flow measurements a single bimolecular step is an inadequate description of the binding mechanism and an additional step is required to accommodate the kinetic data. The rate constants derived from assumed one-step and two-step binding models were determined. The forward rate constants towards the complex formation decrease, and the reverse rate constants increase, with increasing ionic strength. The association rate constants derived from the stopped-flow measurements and the computed diffusional encounter rate constants agree, indicating that the first observed step can be viewed as a diffusionally controlled encounter of the protein and the ligand. Moreover, comparison of experimental and computed bimolecular association rate constants indicate that the experimentally observed decrease of the rate constants with the increasing ionic strength is caused by two factors. The first is less effective steering of the ligand towards the binding site at higher ionic strengths, and the second is that for higher ionic strengths the ligand must be closer to the binding site to induce the fluorescence quenching.

Key words Brownian dynamics · Stopped-flow · Electrostatics · Translation · Protein eIF4E

E. Błachut-Okrasińska · E. Bojarska · A. Niedźwiecka
L. Chlebicka · E. Darżynkiewicz · R. Stolarski · J. Stępiński
J. M. Antosiewicz (✉)
Department of Biophysics,
University of Warsaw, Warsaw 02-089, Poland
E-mail: jantosi@biogeo.uw.edu.pl
Fax: +48-22-8220248

Introduction

The initiation of eukaryotic mRNA translation is a complicated process, involving assembly of a large protein-RNA complex that directs the ribosome to the initiation codon. Messenger RNA is recruited by binding to the 43S initiation complex to form the 48S initiation complex (Merrick and Hershey 1996). *Cis*-acting elements in the mRNA that stimulate this process include the 5′-terminal cap, 7-methylguanosine, connected by a 5′-to-5′ triphosphate bridge to the next nucleotide, 7-methyl-GpppN, where N may be any nucleoside: A, G, C or U (Shatkin 1976). Cap-dependent initiation also requires *trans*-acting factors that include eIF3 and the members of the eIF4F complex: an ATP-dependent RNA helicase eIF4A, eIF4G and a 25 kDa cap-binding protein eIF4E, as reviewed by Sonenberg (1996). Analogues of the mRNA cap have proven very useful in studying eIF4E function in cap-dependent translation. The structure of the complex of murine eIF4E with 7-methyl-GDP was solved by means of X-ray diffraction (Marcotrigiano et al. 1997). A similar structure was obtained for yeast eIF4E complexed with 7-methyl-GDP by means of a multidimensional NMR study (Matsuo et al. 1997). Binding of cap analogues to eIF4E has been followed by quenching of the intrinsic tryptophan fluorescence of eIF4E (see e.g. Carberry et al. 1989), owing to sandwich stacking between 7-methylguanine and two tryptophan indole rings (Marcotrigiano et al. 1997; Matsuo et al. 1997). Spectroscopic emission studies of eIF4E-cap complexes give further insight into the physicochemical basis of the interaction and structural requirements of the cap analogues for their inhibitory properties in translation (Cai et al. 1999). The aim of the present study is to apply stopped-flow measurements and Brownian dynamics (BD) simulations to analyze the rate constants for complex formation between eIF4E and 7-methyl-GpppG.

Materials and methods

Reagents and syntheses

All chemicals for sample preparations and chemical syntheses were of analytical grade, purchased from Roth. The synthesis of 7-methyl-GpppG was performed as described by Darżynkiewicz et al. (1990), and GpppG was synthesized according to Stępiński et al. (1995).

Protein preparation

Murine eIF4E(28-217) was expressed in *Escherichia coli*, strain BL21(DE3)pLysS, transformed with a pET 11d plasmid. The cultures of bacteria were grown in Luria-Berthani broth with ampicillin and chloramphenicol until $OD_{595\,nm} \approx 1.0$, when IPTG was added (0.5 mM) to induce T7 polymerase (Marcotrigiano et al. 1997). The protein was purified from an inclusion bodies pellet and folded by one-step dialysis from 6 M guanidine hydrochloride, followed by anion exchange chromatography on a MonoS column.

Fluorescence measurements and determination of the equilibrium association constant

Fluorescence measurements were carried out on a Perkin-Elmer LS 50B spectrofluorometer, thermostated at 20.0 ± 0.2 °C, the temperature being controlled inside the cuvette with a thermocouple. The cuvette had 4 mm and 10 mm path lengths for absorption and fluorescence, respectively. For all measurements, an excitation slit giving 2.5 nm spectral band width at the excitation wavelength of 280 nm, and an emission slit giving 2.5 or 4.0 nm at 336 or 350 nm, were employed. Fluorescence titrations were performed in 50 mM Hepes-KOH buffer, pH 7.2 ± 0.1, 50, 150 and 350 mM KCl, 0.5 mM EDTA, by adding 1 μL aliquots of 7-methyl-GpppG to a 1400 μL solution of eIF4E. Corrections for dilution (less than 3%) and for the inner filter effect (absorption up to 0.18) were made (Wieczorek et al. 1998). Neglect of the corrections led to the equilibrium association constants within 5% of the values obtained with the corrections. The fluorescence intensity was monitored by means of time-synchronized measurements at the emission wavelength of 336 nm or 350 nm, with an integration time of 40 s, and a gap of 20 s for adding the cap analogue. The equilibrium association constant K was obtained as a parameter of a numerical least-squares nonlinear regression analysis of the fluorescence $F(c_L)$ of eIF4E upon total concentration of the cap c_L, according to the equation:

$$F(c_L) = F(0) - [c_{PL}(\Delta\Phi + \Phi_{FL}) - c_L\Phi_{FL}] \quad (1)$$

where the concentration of the protein-ligand complex, c_{PL}, is given by:

$$c_{PL} = \frac{c_L}{2} + \frac{c_{AP}}{2} + \frac{1}{2K} - \frac{\sqrt{(Kc_L - Kc_{AP} + 1)^2 + 4Kc_{AP}}}{2K} \quad (2)$$

and $\Delta\Phi$ is the difference between the fluorescence efficiencies of the native and complexed protein, Φ_{FL} is the fluorescence efficiency of the free ligand and c_{AP} is the total concentration of the active protein. The final value of K was calculated as a weighted average from five independent titration series for each KCl concentration. $\Delta\Phi$, Φ_{FL} and c_{AP} are also free parameters of the fit.

Stopped-flow measurements

Stopped-flow kinetic measurements were run on a SX.18MV stopped-flow reaction analyzer from Applied Photophysics in the SK1E configuration, which allows for selection of both emission and excitation wavelengths. Emission of eIF4E was excited at 280 nm (slit widths = 1 mm = 4.65 nm), and the fluorescence of the protein was monitored at 335 nm (slit widths = 3 mm). Absorption and emission pathlengths in the stopped-flow cell were 2 mm and 10 mm, respectively. The investigated reactions were initiated by mixing equal volumes of equimolar concentrations of eIF4E and 7-methyl-GpppG at 20 °C, in 50 mM Hepes-KOH buffer, 0.5 mM EDTA, pH 7.2, and 50, 150 and 350 mM KCl. Control experiments were performed with GpppG, which weakly binds to eIF4E. The solutions were filtered prior concentration determination and subsequently degassed before placing them into the stopped-flow syringes. One thousand data points were recorded over the course of each reaction using an oversampling option of the instrument, and over 100 runs were averaged for each concentration of the reagents. Concentrations of the reagents were determined spectrophotometrically using $\epsilon_{280\,nm} = 53{,}400\ M^{-1}\,cm^{-1}$ for the protein at pH 7.2, $\epsilon_{280\,nm} = 14{,}000\ M^{-1}\,cm^{-1}$ for 7-methyl-GpppG and $\epsilon_{280\,nm} = 15{,}000\ M^{-1}\,cm^{-1}$ for GpppG. The average fraction of the active protein resulting from more than 50 independent titration series was $57 \pm 16\%$ (see previous section). The concentrations of the reagents, as determined by absorption measurements, covered the range of 0.1–4.1 μM in the apparatus syringes. This is well below the concentration range where any problems with the protein aggregation can be expected (Marcotrigiano et al. 1997).

Analysis of the stopped-flow data

Kinetic traces were analyzed using a 4.34 version of the Applied Photophysics SX.18MV kinetic spectrometer workstation software. The fluorescence decrease accompanying the binding of 7-methyl-GpppG to eIF4E was analyzed in terms of both one-step and two-step models:

$$P + L \underset{k_D}{\overset{k_R}{\rightleftharpoons}} (PL) \quad \text{and} \quad P + L \underset{k_{-1}}{\overset{k_{+1}}{\rightleftharpoons}} (PL) * \underset{k_{-2}}{\overset{k_{+2}}{\rightleftharpoons}} (PL) \quad (3)$$

where $k_R = k_{+1}k_{+2}/(k_{+2} + k_{-1})$ and $k_D = k_{-1}k_{-2}/(k_{+2} + k_{-1})$ for the steady-state condition. Rate constants for both mechanisms were derived from the well-known relations between the relaxation times τ, obtained from the kinetic traces, and the equilibrium concentrations of the free protein $\bar{c}_P$ and the cap analogue $\bar{c}_L$ (Bernasconi 1976; Eigen and De Maeyer 1974). For the one-step process the following relation holds:

$$1/\tau = k_R(\bar{c}_P + \bar{c}_L) + k_D \quad (4)$$

which requires an a priori knowledge of the equilibrium association constant K of the process. On the other hand, for the two-step process, four rate constants were derived from the following relations:

$$\frac{1}{\tau_1} = k_{+1}(\bar{c}_P + \bar{c}_L) + k_{-1} \quad (5)$$

and

$$\frac{1}{\tau_2} = \frac{k_{+2}k_{+1}}{k_{-1}} \frac{\bar{c}_P + \bar{c}_L}{1 + (\bar{c}_P + \bar{c}_L)(k_{+1}/k_{-1})} + k_{-2} \quad (6)$$

which are valid when the first step equilibrates much more rapidly than the other. It seems that the system investigated in the present study partially fulfills this condition, as the observed dependences of $1/\tau_1$ and $1/\tau_2$ are close to the functional forms presented by Eqs. (5) and (6). For the two-step process, four rate constants can also be derived from the following relations:

$$\frac{1}{\tau_1} + \frac{1}{\tau_2} = k_{+1}(\bar{c}_P + \bar{c}_L) + k_{-1} + k_{+2} + k_{-2} \quad (7)$$

and

$$\frac{1}{\tau_1} \cdot \frac{1}{\tau_2} = k_{+1}(\bar{c}_P + \bar{c}_L)(k_{+2} + k_{-2}) + k_{-1}k_{-2} \quad (8)$$

which do not depend on any assumption regarding the speed of equilibration of both steps. However, it should be noted that when τ_1 and τ_2 are not different by a factor of at least 5, the utility of Eqs. (5), (6), (7) and (8) is limited.

Structures used in calculations

Calculations were based on the crystal structure of truncated murine eIF4E (28-217) (Marcotrigiano et al. 1997). Figure 1 presents a ribbon model of eIF4E complexed with 7-methyl-GDP shown in a CPK representation. The residues important for the ligand binding and directly involved in fluorescence quenching are shown in the stick representation, and are labelled by the names and residue numbers in the eIF4E sequence. The coordinate file of Marcotrigiano et al. (1997) contains hydrogen atoms. For the purpose of calculations in this paper, all hydrogen coordinates were stripped from the protein coordinates data set and subsequently all polar and aromatic rings hydrogens were added using a HBUILD command of CHARMm (Brunger and Karplus 1988). Their orientations were subsequently optimized with CHARMM (Brooks et al. 1983).

An all-atom model of 7-methyl-GpppG was prepared using the Biopolymer module of the InsightII Molecular Modeling software (Molecular Simulations 1992b). It is known that the two guanine bases of 7-methyl-GpppG participate in internal stacking interactions (Wieczorek et al. 1997). However, in the complex with the protein the ligand is in an extended form. Unfortunately, the present simulation algorithm used by us does not allow inclusion of such extensive conformational changes in the ligand. Therefore, the model was constructed in an extended conformation and refined subsequently in 500 steps of energy minimization.

The atomic models of the protein and the ligand were used to construct their electrostatic and hydrodynamic models in the Poisson-Boltzmann and BD simulations, as described below.

Hydrodynamic models of the protein and the ligand

The protein and ligand are modelled by sets of spherical beads so that their shapes are close to reality. In such models the appropriate diffusion tensors, which take into account hydrodynamic interactions (Yamakawa 1970) between subunits of the given molecule, are calculated as described in detail elsewhere (Antosiewicz and Porschke 1989; Garcia de la Tore and Bloomfield 1981).

In the case of the protein, each amino acid is substituted by one bead. The common radius of the beads (4.6 Å) reflects an average size of the residues, and includes additionally 1.4 Å to take into account the hydration layer. Such a procedure leads to the computed average translational diffusion coefficients of proteins in reasonable agreement with the experimental data (Antosiewicz 1995). The computed average translational diffusion coefficient of eIF4E is 9.97×10^{-7} cm^2/s at 20 °C, which is equivalent to a sphere of radius of 21.5 Å.

In the case of the ligand, each atom is initially substituted by one 1.2 Å bead. Such a representation leads to a reasonable agreement of the measured and computed translational diffusion coefficients for small molecules (Antosiewicz et al. 1995). The computed average translational diffusion coefficient of 7-methyl-GpppG is 3.44×10^{-6} cm^2/s, which is equivalent to a 6.2 Å sphere. The association rate constant for uniformly reactive, but electrically neutral, spheres with the radii given above, predicted by the Smoluchowski theory (von Smoluchowski 1917), is 9.2×10^9 M^{-1} s^{-1}. This gives us some reference for the measured and computed association rate constants in this paper. Subsequently, 7-methyl-GpppG is represented by a five-sphere model. The positions of the beads were calculated as follows. The first and the fifth beads are situated at the geometric centers of G and 7-methyl-G, respectively. The second and the fourth beads are positioned at the geometric centers of both phosphoriboses, and the third bead is located at the geometric center of the second phosphate group. The common radius of these five beads was assigned a value of 3.3 Å, which gives for the resulting five-bead model the same average translational diffusion coefficient as that computed for the all-atom-based hydrodynamic model. The distances between the ligand beads can change within ±0.1 Å; therefore the model exhibits some degree of flexibility.

Figure 2 shows the resulting bead models of eIF4E and 7-methyl-GpppG. By such modelling we have accurately estimated the relative diffusion coefficients, provided that hydrodynamic interactions between the protein and the ligand can be neglected. We are forced to do so, because calculations with the hydrodynamic interactions between 183 subunits of the protein and 5 subunits of the ligand, required in the present case, are too computationally demanding for present-day computers. It is difficult to estimate how large would be the decrease of the calculated rate constants for a detailed hydrodynamic model of protein-ligand interactions while it depends on many details (Deutch and Felderhof 1973; Friedman 1966). Recent simulations (Antosiewicz and McCammon 1995) for a dumbbell protein and a dumbbell ligand model showed that computations neglecting the protein-ligand hydrodynamic interactions, for stick boundary conditions for the solvent velocity on the surfaces of moving particles, lead to rate constants which are 27–32% too high in comparison to the simulations which include these interactions.

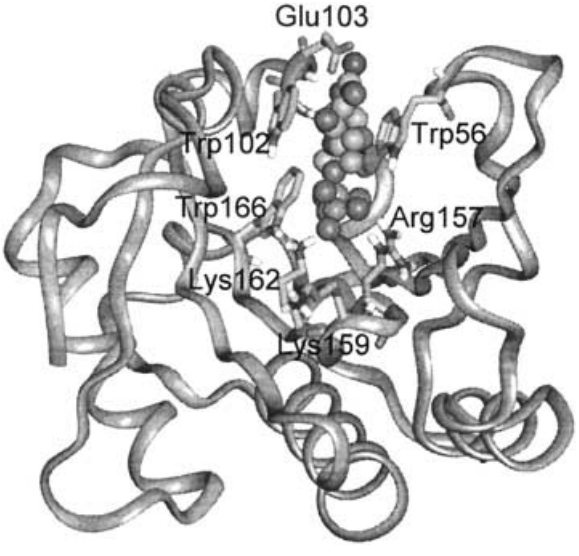

Fig. 1 Structure of murine eIF4E complexed with 7-methyl-GDP, showing the amino acids involved in the binding of the ligand

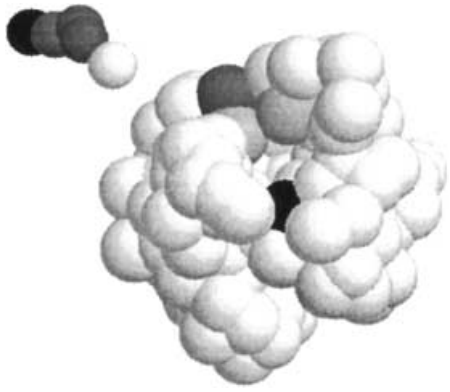

Fig. 2 Five-bead model of 7-methyl-GpppG and hydrodynamic model of the protein used in Brownian dynamics simulations. Several beads are marked: the *black beads* correspond to positive charges (that of the 7-methyl-G of the ligand and Lys162 of the protein), the *dark grey beads* correspond to negative charges (phosphate beads of the ligand and Glu103 of the protein), and the *light grey beads* correspond to Trp56 and Trp102, participating in the interactions with 7-methyl-G

Electrostatic models of the protein and the ligand

BD simulations described below require that electrostatic interactions (EI) between the associating molecules are included. In the case of molecules like proteins and nucleic acids, the electrostatic properties are determined to a large extent by the ability of nucleotides and certain amino acids to exchange protons with their environment, and the dependence of these processes on pH. Charge distribution in eIF4E, corresponding to experimental conditions in the stopped-flow measurements, was calculated by our computer methodology for titration of proteins, as described in full detail elsewhere (Antosiewicz et al. 1996; Briggs and Antosiewicz 1999). Our approach is based on the assumption that the difference in protonation behavior of a given group, in the isolated amino acid and in the protein environment, results exclusively from the differences in electrostatic interactions in the two situations. The required electrostatic calculations were performed using the finite-difference Poisson-Boltzmann (PB) method (Warwicker and Watson 1982). The PB model for macromolecular electrostatics treats the solute as a low-dielectric region bounded by the molecular surface, and containing atomic charges. The charges are located at the atomic positions determined, for example, by X-ray crystallographic methods. The solute is surrounded by high-dielectric aqueous solvent which may contain a dissolved electrolyte. All finite-difference calculations required by our procedures (Antosiewicz et al. 1996) were carried out using the UHBD program (Madura et al. 1995).

In the current BD methodology employed here, charges of the ligand molecule are treated as a set of trial charges. Hence, 7-methyl-GpppG is treated in a simplified way: unit elementary charges are assigned to the beads representing its hydrodynamic model. The bead corresponding to 7-methylguanine has a positive elementary charge, each of the three beads containing a phosphate group has –1 elementary charge, and the bead corresponding to the unmethylated guanine base is uncharged.

BD methods

Simulations of molecular diffusion and calculation of the rate constant for the diffusion-controlled encounter between eIF4E and 7-methyl-GpppG are based on the BD method (Ermak and McCammon 1978; Northrup et al. 1984). BD simulations were done using the UHBD program (Madura et al. 1995). One computes and then analyzes many trajectories of one reactant diffusing toward its partner under the influence of electrostatic intermolecular forces and the random forces mimicking the influence of the bombardment by the solvent molecules. The latter forces are modelled by generating random numbers from a Gaussian distribution and using estimated diffusion coefficients of the molecules. The electrostatic forces are modelled by computing the electrostatic potential generated by the protein and treating the ligand as a set of trial charges moving in the field created by the protein. Trajectories are initiated on the surface of a sphere of radius r_b, the b-surface, around the center of coordinates of the protein. This sphere is made sufficiently large so that the electrostatic forces between the protein and the ligand are approximately centrosymmetric for $r > r_b$. Each trajectory is continued until the ligand satisfies a predefined encounter criterion or reaches an outer spherical surface of radius r_q, the quit sphere. The fraction of trajectories that finish with encounters, β_b, is corrected to include the additional encounters that would have occurred if the trajectories had not been truncated at the quit surface. It is then multiplied by the rate constant for the encounter of the ligand with the b-surface to yield the bimolecular diffusion-controlled rate constant k_d (Davis et al. 1991; Madura et al. 1995). This is summarized in the following equations

$$k_d = k_b \frac{\beta_b}{1 - (1 - \beta_b)\frac{k_b}{k_q}} \tag{9}$$

where, in general (Friedman 1966; Kramers 1940):

$$k_{b(q)} = 4\pi \left[\int_{r_{b(q)}}^{\infty} \frac{e^{U(r)/kT}}{r^2 D_w(r)} dr \right]^{-1} \tag{10}$$

and $U(r)$ is a centrosymmetric potential of interaction between molecules, and $D_w(r)$ is a distance-dependent relative translational diffusion coefficient.

Parameters and other details of the simulations

All simulations were performed at 293 K ($RT = 0.58$ kcal/mol), at ionic strengths equivalent to 50, 100, 150, 250 and 350 mM monovalent salt, with the solvent dielectric constant of 80, and that of the protein of 4. The dielectric boundary between the protein and the solvent is defined as a Richards probe-accessible surface (Richards 1977) with a 1.4 Å probe radius, and an initial set of 280 surface dots per atom (Gilson et al. 1988). All atomic partial charges and radii for the protein were taken from the CHARMM22 parameter set for the standard amino acids (Brooks et al. 1983; Molecular Simulations 1992a).

Electrostatic potential around the protein was generated on a 100^3 cubic grid with a 1.0 Å spacing. The b-sphere radius was 65 Å, and the q-radius was 300 Å. In order to account for steric exclusion of the ligand by the protein, the center of any bead of the ligand was not allowed to come closer than 2 Å to the van der Waals surface of any protein atom. This rather small exclusion radius attempts to crudely account for the conformational fluctuations of the protein binding site, making the encounter criteria (see below) easier to satisfy.

We used variable time steps in the BD simulations: for the ligand closer than 42 Å to the center of eIF4E the time step was set to 0.03 ps, between 42 and 100 Å it was set to 0.15 ps, and above 100 Å it was set to 0.30 ps.

As a reference, simulations which neglect the electrostatic interactions between protein and ligand were also performed. Diffusional rate constants reported in the present work are based on 90,000 Brownian trajectories.

The encounter or complex formation criteria for the BD simulations were established as follows. First, the 7-methyl-GDP complexed with eIF4E (Marcotrigiano et al. 1997) was modelled by three spherical beads in the analogous way as 7-methyl-GpppG was modelled by five beads. These three beads are equivalent to the first three beads of the 7-methyl-GpppG model. The center of the 7-methyl-G bead in the crystal structure of the eIF4E-7-methyl-GDP complex is located 5.4 Å from the CD atom [the name follows PDB file nomenclature (Bernstein et al. 1977)] of Glu103 and 3.8 Å from the CH2 atom of Trp102, and the bead corresponding to the second phosphate is located 3.6 Å from the NZ atom of Lys162. These three distances define the three corresponding "reaction" distances in the final complex. For the purpose of BD simulations, these three distances were increased to 6, 5 and 5 Å, respectively, just to increase the probability of formation of the complex. Moreover, because it is not known at which distance of the ligand from its binding site the quenching of the protein fluorescence starts, several less restrictive criteria were also used, and we increased all three encounter distances at 1 Å steps, ending with 11, 10 and 10 Å. All the encounter criteria are given in Table 4, which also reports the results of the BD simulations.

Results

Equilibrium association constants

A typical example of the fluorescence titration, giving the equilibrium association constant, is illustrated in Fig. 3. Table 1 presents the equilibrium association

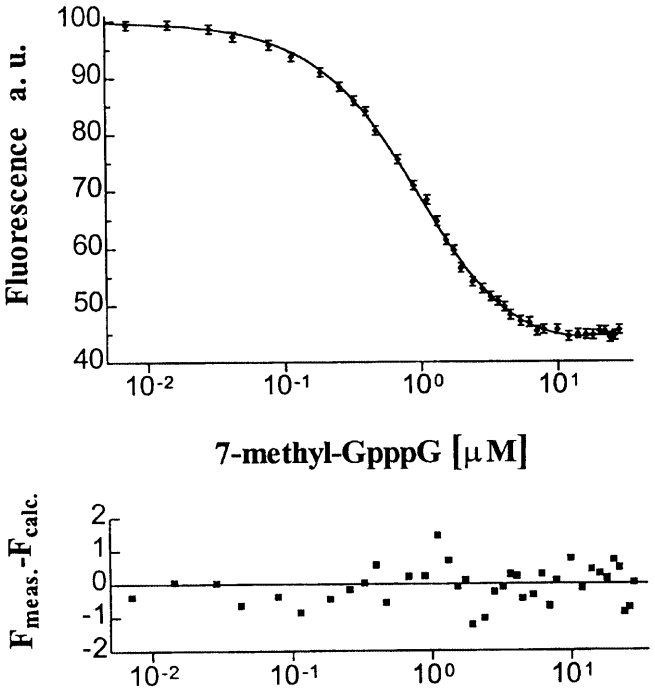

Fig. 3 Intrinsic fluorescence quenching of eIF4E due to association with 7-methyl-GpppG (*top*) and the accuracy of fitting of the theoretical relationship [Eq. (1)] to the experimental data points (*bottom*)

constants at three ionic strengths applied for the kinetic studies. The equilibrium constants were subsequently used in calculations of the sum of the equilibrium concentrations of free protein and free ligand, $\bar{c}_P + \bar{c}_L$, for experimentally determined rate constants, according to Eqs. (4), (5), (6), (7) and (8), with the total concentration of the protein taken as 60% of the concentration determined from UV absorption, in accordance with analysis of the steady-state fluorescence measurements [see Eq. (1) in Materials and methods]. Such an approach leads to consistency between equilibrium association constants from stopped-flow measurements, determined as k_R/k_D with those obtained from the fluorescence titrations.

Relaxation times and amplitudes from stopped-flow experiments

As is well known, formation of a complex between eIF4E and 7-methyl-GpppG leads to a decrease of the intensity of fluorescence, owing to quenching processes (Carberry et al. 1989). Figure 4 shows examples of kinetic traces obtained after mixing of eIF4E with 7-methyl-GpppG, and for comparison, with non-binding GpppG. Relaxation times and relative relaxation amplitudes obtained with assumption of single-step and two-step association reactions are summarized in Tables A1, A2, and A3 in the Appendix. Concentrations in Tables A1, A2, and A3 were obtained from absorption measurements and refer to their values in the stopped-flow apparatus syringes. However, $\bar{c}_P + \bar{c}_L$ were calculated assuming that the actual concentration of the active protein, participating in the binding, is 60% of the indicated values (see the subsection Stopped-flow

Fig. 4 Comparison of the fluorescence time dependence on mixing of eIF4E with 7-methyl-GpppG (*decaying trace*, the average of 168 shots), shown with the two-relaxation fit, and with GpppG (*flat trace*, the average of 56 shots). The *insert* shows the initial stages of both traces. The difference between the flat trace and the beginning of the decaying trace indicates the extent of binding, which occurs during the dead time of the stopped-flow instrument (ca. 1.2 ms). The experimental conditions were as follows: excitation at 280 nm, fluorescence observation at 335 nm, temp. 20 °C, 350 mM KCl, pH 7.2, initial concentrations of the protein and ligand 2.9 μM (in the syringes, protein concentration before correction for active protein)

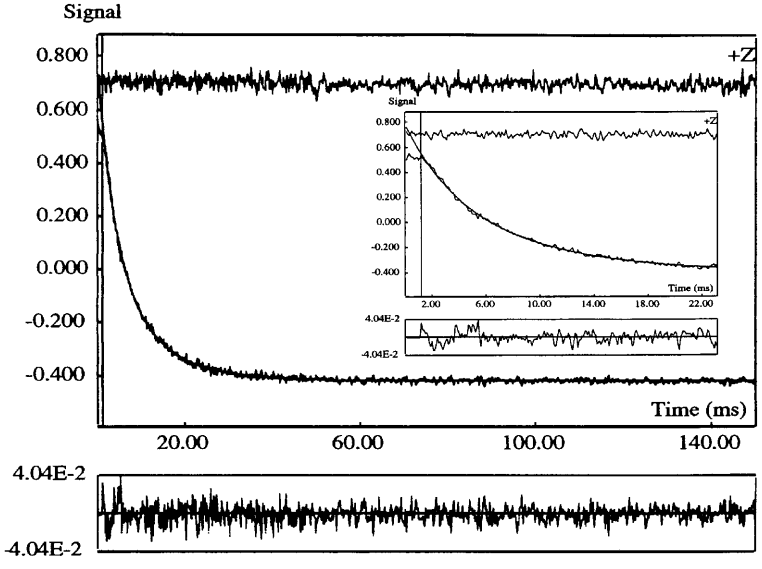

Table 1 Equilibrium association constants K for the eIF4E-7-methyl-GpppG complex, at 293 K, in 50 mM Hepes-KOH buffer, pH 7.2, at indicated concentrations of added KCl. The buffer adds to the ionic strength an equivalent of ca. 33 mM monovalent salt

Added KCl (mM)	K (10^6 M^{-1})
50	16.1 ± 0.5
150	4.4 ± 0.3
350	0.9 ± 0.3

measurements). The last columns of Tables A1, A2, and A3 indicate relative increase in accuracy of the fit, if instead of a single step process a two-step process is assumed. It can be clearly seen that for most cases the assumption of two relaxation processes leads to a statistically significant improvement of the fits. The errors in Tables A1, A2, and A3 are standard errors given by the kinetic spectrometer workstation software. Reproducibility of the relaxation times and amplitudes with samples coming from independent preparations indicate that the statistical error is about ± 15–20% of the measured value, but not less than ± 5 s^{-1} for the inverse of relaxation time and ± 0.04 for the relative amplitude.

Relaxation times presented in Tables A1, A2, and A3 are shown in Figs. 5, 6, 7 as functions of $\bar{c}_P + \bar{c}_L$. It can be seen that the relaxation times resulting from single-relaxation fits satisfy the linear relation to $\bar{c}_P + \bar{c}_L$ according to Eq. (4) pretty well (see Fig. 6). The two relaxation times obtained from dual fits are not so well compatible with the relations predicted by Eqs. (5) and (6) (see Fig. 6), and Eqs. (7) and (8) (see Fig. 7). This apparently results from difficulties with accurate estimation of the two relaxation times when they are not well separated and/or because we are dealing with a spectrum of the relaxation processes rather than two separate steps.

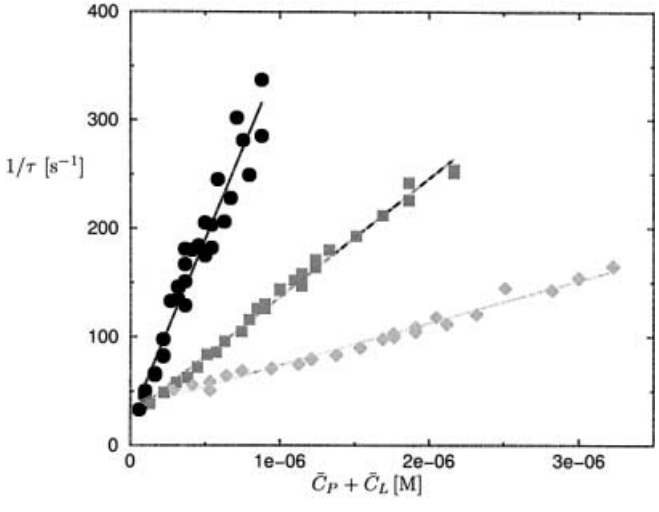

Fig. 5 Dependence of the inverse of the single-fit relaxation times on the sum of the equilibrium concentrations of the free protein and ligand, for different amounts of added KCl (in mM) to 50 mM Hepes-KOH buffer, pH 7.2: *filled circles* for 50 mM, *filled squares* for 150 mM and *filled diamonds* for 350 mM

Experimental rate constants

Two overall rate constants, k_R and k_D, obtained from the present experimental data are shown in Table 2. It should be noted that the overall equilibrium constants calculated from the ratio of k_R and k_D agree well with

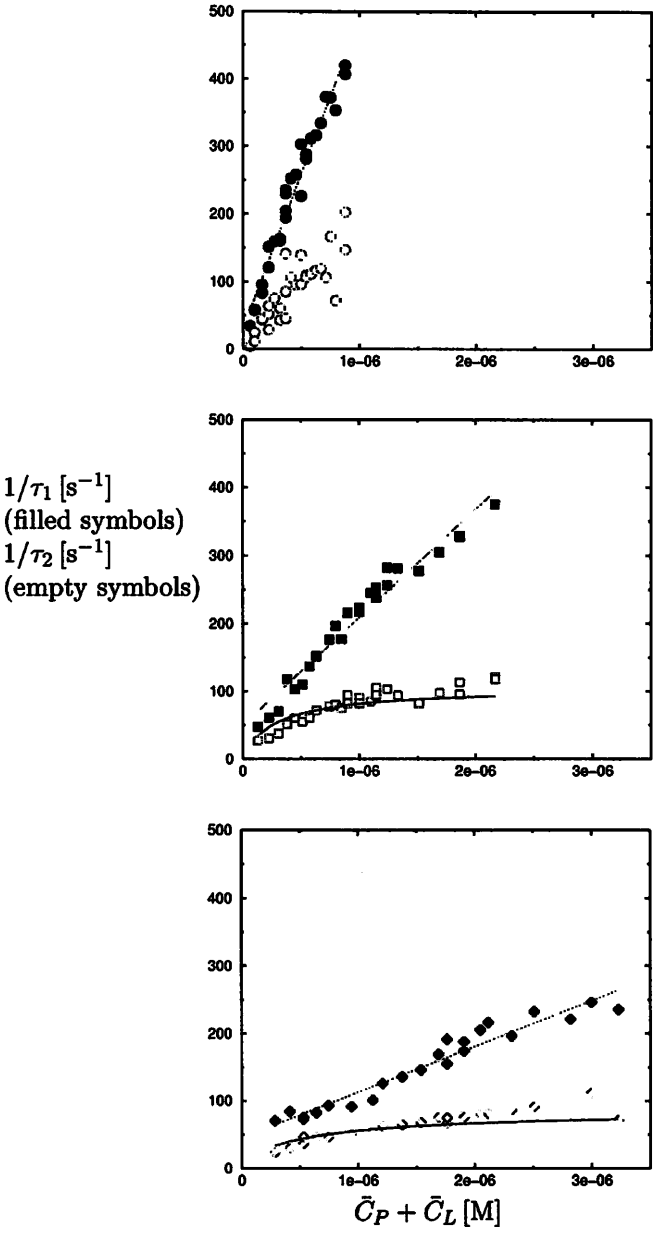

Fig. 6 Dependence of the inverse of the shorter relaxation time (*filled symbols*) and of the longer relaxation time (*open symbols*) on the sum of the equilibrium concentrations of the free protein and ligand for different amounts of added KCl (in mM) to 50 mM Hepes-KOH buffer, pH 7.2: *circles* for 50 mM, *squares* for 150 mM and *diamonds* for 350 mM

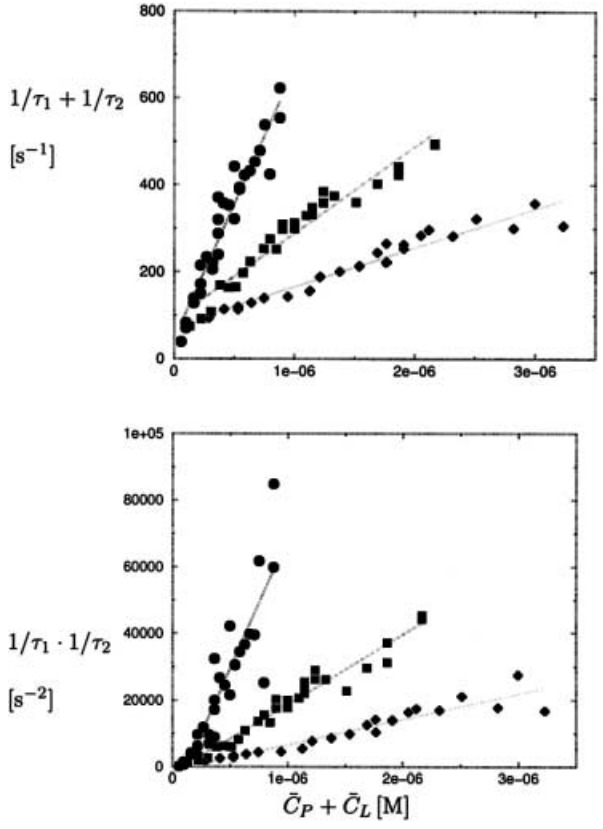

Fig. 7 Dependence of the sum (*top*) and the product (*bottom*) of the inverse shorter and longer relaxation times on the sum of the equilibrium concentrations of the free protein and ligand, for different amounts of added KCl (in mM) to 50 mM Hepes-KOH buffer, pH 7.2: *circles* for 50 mM, *squares* for 150 mM and *diamonds* for 350 mM

the equilibrium constants K, determined in the stationary experiments (Table 1). It can be seen that the overall rate constant for the association between eIF4E protein and 7-methyl-GpppG decreases significantly with increasing ionic strength. On the other hand, the overall rate constant for the dissociation process is only slightly dependent on the ionic strength. However, for most cases, dual relaxation fits are significantly better than the corresponding single fits, and therefore the two-step association model was also considered, regardless of the fact that our experimental data do not follow exactly the predictions made by Eqs. (4)–(8). The four rate constants are also shown in Table 2, and they are estimated by the following procedure.

First, from linear regression fits according to Eq. (5) the rate constants k_{+1} and k_{-1} were obtained. Second, the ratio of the slopes of the linear relations predicted by Eqs. (8) and (7), and shown in Fig. 7, gave estimates of $k_{+2}+k_{-2}$ as 125 ± 12 s^{-1}, 105 ± 7 s^{-1} and 85 ± 8 s^{-1} for the three concentrations of added KCl, i.e. 50, 150 and 350 mM, respectively. These values agree well with the averages of the last 5–7 values of $1/\tau_2$ as functions of $\bar{c}_P + \bar{c}_L$ shown in Tables A1, A2, and A3; therefore they seem reliable. The next step was to estimate individual values of k_{-2} and k_{+2}. However, this is difficult because our experimental relaxation times τ_1 and τ_2 are not well separated. On the one hand, extrapolation of $1/\tau_2$ towards zero values of $\bar{c}_P + \bar{c}_L$ suggests that the k_{-2} values are very small. On the other hand, from the relation $K \equiv k_R/k_D = (k_{+1}/k_{-1})(k_{+2}/k_{-2}) \equiv K_1 K_2$ and the estimated ratios of the equilibrium constants K/K_1 for different amounts of added KCl (see Table 2), we can conclude that the values of k_{-2} and k_{+2} cannot differ too much. Because of these discrepancies, we estimated the values of k_{-2} and k_{+2} from one-parameter fits to the modified Eq. (6) in the form:

$$\frac{1}{\tau_2} = K_1 \cdot (k_{-2} + k_{+2} - A0) \cdot \frac{\bar{c}_P + \bar{c}_L}{1 + K_1(\bar{c}_P + \bar{c}_L)} + A0 \qquad (11)$$

where $A0$ is the adjustable parameter which has the meaning of an individual value of k_{-2}. The restrictions imposed on the adjustable parameter were $A0 \geq 1$. Figure 6 presents linear plots for $1/\tau_1$ data according to Eq. (5) and one-parameter plots for $1/\tau_2$ data according to Eq. (11). For 150 and 350 mM of added KCl the latest procedure leads to reasonable estimates of k_{-2}. For 50 mM of added KCl the scatter of the data is too large and the the fit is not good even for $A0 = 1$. Therefore for this experimental condition, k_{+2} and k_{-2} were roughly estimated as 124 and 1 s^{-1}, respectively. All the data resulting from stopped-flow experiments are presented in Table 2. Although estimation of individual values of k_{-2} and k_{+2} can be only treated as semiquantitative, we think that these data allow a conclusion that k_{-2} increases, and k_{+2} decreases, with an increase of the ionic strength. This is a similar dependence as observed for k_R and k_D and for k_{+1} and k_{-1}.

Table 2 Rate constants for association and dissociation of the eIF4E protein and 7-methyl-GpppG obtained from single- and from dual-relaxation fits to the kinetic traces registered during the stopped-flow experiments at 293 K, in 50 mM Hepes-KOH buffer, pH 7.2, at indicated concentrations of added KCl. The buffer adds to the ionic strength an equivalent of 33 mM monovalent salt. The rate constants for the second step are given without error estimates, as they are derived in a rather heuristic way, using one-parameter least-squares fits according to Eq. (11)

Concentration of added KCl (mM)	Single fit		Dual fit			
	k_R (10^8 M^{-1} s^{-1})	k_D (s^{-1})	k_{+1} (10^8 M^{-1} s^{-1})	k_{-1} (s^{-1})	k_{+2} (s^{-1})	k_{-2} (s^{-1})
50	3.33 ± 0.17	24 ± 8	4.58 ± 0.18	30 ± 8	124	1
150	1.09 ± 0.02	28 ± 3	1.59 ± 0.07	50 ± 8	99	6
350	0.39 ± 0.01	35 ± 2	0.68 ± 0.04	45 ± 7	73	12

Table 3 Predicted electrostatic properties of eIF4E at 293 K, pH 7.2, as a function of ionic strength

Ionic strength (mM)	Average charge (e)	Mean dipole moment (D)
50	0.56	571
100	0.58	579
150	0.58	585
250	0.58	591
350	0.58	595

Diffusional encounter rate constants from BD simulations

The predicted average charges of eIF4E at pH 7.2 and its mean dipole moments are given in Table 3 as functions of the ionic strength. Both the charge and the dipole moment are rather insensitive to the ionic strength. Our calculations predict that eIF4E at pH 7.2, and at ionic strengths corresponding to 50–350 mM KCl, should have an average charge of +0.6 units of elementary charge, and an average dipole moment of 600 D units. Thus it can be expected that electrostatic steering plays some role in the association process.

Computed diffusional encounter rate constants [Eqs. (9) and (10)] as functions of the ionic strength, for different encounter criteria, are given in Table 4. This table presents also the rate constants computed when electrostatic interactions are neglected. It can be noted that the range of presented values, with the electrostatic interactions included, agree with the experimental evaluations of k_{+1} given in Table 2. The electrostatic interactions introduce approximately fivefold (for 50 mM) to twofold (for 350 mM) acceleration of the rate of association.

Discussion

The present study provides estimates of the rate constants which characterize association of murine eukaryotic translation factor eIF4E with a cap analogue, 7-methyl-GpppG. Analysis of experimental data in terms of one relaxation process is useful because it provides us with accurate estimates of average values of kinetic parameters characterizing processes for formation of the molecular complexes. Ionic strength dependences of k_R and k_D agree with expectations based on electrostatic considerations. Screening of the electrostatic interactions should lead to slower rates of association of electrostatically interacting partners of the encounter and to make easier separation of electrostatically interacting molecules in the complex. Also the screening should be much more effective for the association process than for the dissociation of the complex because in the complex the solvent is removed from some part of the molecular surface. Accordingly, the ionic strength effects should be more pronounced for k_R and much smaller for k_D.

In the previous section it was shown that single relaxation is not sufficient to explain kinetic traces observed in the stopped-flow experiments consisting of mixing the cap binding protein eIF4E with the analogue of the 5′-end cap of mRNA, 7-methyl-GpppG. Unfortunately, despite an enormous number of experimental data, large numbers of concentrations and very large numbers of traces averaged for each concentration, our two relaxation fits do not lead to dependencies of relaxation times on concentrations which exactly agree with Eqs. (5), (6), (7) and (8). Consequently, our evaluations of all four rate constants, accompanying the two relaxation processes, are not highly accurate. Nevertheless, they can be treated as useful estimates. Our BD simulations gave the rate constants k_d in good agreement with the k_{+1} obtained from the stopped-flow measurements. Therefore, the faster relaxation process can be attributed to the entering of the ligand to the binding site pocket of the protein and its speed is limited by diffusion processes. A large value of the measured rate constant k_{+1} does not necessarily mean diffusional control and the results of BD simulations are helpful at this point. Different factors, like geometry and size of the protein's binding site and electrostatic and hydrodynamic interactions, can change diffusional encounter

Table 4 Computed diffusional association rate constants k_d (units 10^8 M^{-1} s^{-1}) for 7-methyl-GpppG and eIF4E protein, at 293 K, pH 7.2, as a function of the ionic strength of the solution and various distance criteria for complex formation. Encounter criteria are defined as distances between the following three pairs of protein atoms and the ligand subunits: 7-methyl-G-CD(Glu103), 7-methyl-G-CH2(Trp102) and P2-NZ(Lys162), being not greater than indicated values in Ångstrom units. EI refers to electrostatic interactions, and indicated errors refer to the 90% confidence level

Encounter distances (Å)	Electrostatic model in calculations					
	Ionic strength					No EI
	50	100	150	250	350	
11/10/10	4.18 ± 0.18	4.01 ± 0.18	3.63 ± 0.17	3.36 ± 0.17	3.30 ± 0.17	1.89 ± 0.13
10/9/9	3.26 ± 0.16	3.23 ± 0.16	2.76 ± 0.15	2.61 ± 0.15	2.58 ± 0.15	1.40 ± 0.11
9/8/8	2.30 ± 0.14	2.28 ± 0.14	2.00 ± 0.13	1.81 ± 0.12	1.81 ± 0.12	0.85 ± 0.08
8/7/7	1.30 ± 0.10	1.23 ± 0.10	1.15 ± 0.10	1.01 ± 0.09	1.00 ± 0.09	0.47 ± 0.06
7/6/6	0.80 ± 0.08	0.78 ± 0.08	0.71 ± 0.08	0.64 ± 0.07	0.58 ± 0.07	0.26 ± 0.05
6/5/5	0.38 ± 0.06	0.35 ± 0.05	0.32 ± 0.05	0.29 ± 0.05	0.25 ± 0.05	0.08 ± 0.03

rate constants by 2–3 orders of magnitude. The slower relaxation processes relate to internal changes in the protein-ligand complex. However, comparison of experimental and computed association rate constants leads to one more interesting observation.

When we compare the experimental values of k_D with the computed values of k_d, it can be noted that fluorescence quenching is completed before the ligand comes to its final position in the binding site. For an ionic strength of 350 mM it occurs ca. 1 Å apart from its position in the crystal structure, for an ionic strength of 150 mM it occurs 2 Å above it, and for an ionic strength of 50 mM it occurs 5 Å above this point. Similar observations can be made when we compare the experimental value of k_{+1} and the computed k_d. The agreement between the computed and experimental diffusional encounter rate constants occurs for even larger distances. This leads to the conclusion that the observed decrease of the association rate constant with increasing ionic strength is due to two factors. The first is that electrostatic steering towards the binding site is less effective and the second is that for larger ionic strengths the ligand must be closer to the binding site to induce the fluorescence quenching. This points to the important role of electrostatic interactions in fluorescence quenching. The most probable mechanism of fluorescence quenching is the formation of a dark complex of the molecules, i.e. static quenching dominates (Lakowicz 1983). However, because of rather small overlapping of the protein emission and the cap analogue absorption spectra, possible participation of resonance energy transfer of the Förster type would be of less importance. Even if the resonance transfer does occur, the energy is quickly dissipated as we observe neither fluorescence enhancement of 7-methylguanine nor any bathochromically shifted emission band of the Trp56/7-methyl-G/Trp102 heteroexcimer.

Stopped-flow experiments with p28, a functional analogue of eIF4E from wheat germ initiation factor eIF-(iso)4F, and 7-methyl-GpppG were reported previously (Sha et al. 1995). These authors have estimated k_{+2} as 12.2 s^{-1} for the eIF-(iso)4F initiation complex bound with 7-methyl-GpppG, and 123.5 s^{-1} for the binding with the subunit p28, at 100 mM KCl and 23 °C. The latter is in very good agreement with results obtained in the present work for 50 and 150 mM KCl (see Table 2).

Based on the presented experimental and theoretical results, it seems that any more detailed conclusions regarding the mechanism of association of the eIF4E protein with the cap analogue 7-methyl-GpppG would not be justified. However, the presented combined experimental and theoretical study can be extended in several ways and more detailed analysis might be possible. The simplest extension is consideration of additional models of dinucleotide cap analogues like GpppG, and 7-methyl-GpppG-7-methyl, and mononucleoitde cap analogues like 7-methyl-GMP, -GDP and -GTP. Even keeping the theoretical approach at the same level of resolution, one can obtain further significant insights into the understanding of this association process, particularly regarding interpretation of the two association steps concluded from the present study. A second aspect is inclusion of the protein's binding site flexibility during BD simulations (Wade et al. 1993), or even a combination of BD simulations of the diffusional encounter with more detailed molecular dynamics simulations of subsequent events, see e.g. Luty et al. (1993). Another aspect is related to protonation equilibria within the binding site and the ligand. In this respect, pK_a values of Glu103 on the eIF4E and N1 on the 7-methylguanine of the ligand are the most interesting. The pK_a of N1 in a free 7-methyl-GpppG was determined spectrophotometrically as 7.35 ± 0.06 at 20 °C at an ionic strength of 150 mM (Wieczorek et al. 1995). The pK_a of Glu103 in an unliganded eIF4E, computed in the present work, is 5.5; unfortunately there is no experimental data for comparison. In the complex, the N1 of the 7-methylguanine and Glu103 are in close proximity, and their pK_a values are certainly affected. Such extension requires that our computer methodology for predicting protonation equilibria in proteins (Antosiewicz et al. 1996) is developed towards including also nucleic acids and their constituents.

Acknowledgements This work was supported by the Human Frontier Science Program RG0303/1998-M (grant to S.K.Burley, N. Sonnenberg and E.D.), the Polish Committee for Scientific Research (KBN) 6 P04A 055 17 and the U.S.-Poland Maria Sklodowska-Curie Joint Fund II MEN/NSF-98-337. We thank Dr. S.K. Burley and Dr. N. Sonenberg for useful discussions and the coordinates of the eIF4E-7-methyl-GDP complex, J. Marcotrigiano for originating the purification protocol for fully active apoprotein, and Dr. A.-C. Gingras for the plasmid. We also acknowledge the help of Dr. S. Senior of Applied Photophysics with problems we encountered during the stopped-flow measurements, and we thank Dr. Maciej Geller for his help with constructing the atomic model of 7-methyl-GpppG using InsightII software. The stopped-flow reaction analyzer was purchased using funds provided by the Polish Committee for Scientific Research (KBN, 2395/IA/115/97). Diffusional coefficients were calculated using facilities of the Gesellschaft für wissenschaftliche Datenverarbeitung, Göttingen, Germany. All the remaining simulations were done on an O2 SGI workstation purchased using funds of the Fogarty NIH Award TW00768 (J.M.A. and J.A. McCammon of the University of California at San Diego, USA). All plots and the least-squares fits were done using program Xmgr (Evgeny Stambulchik, Rehovot, Israel).

Appendix

Tables

Tables A1, A2 and A3 are a summary of experimental results (relaxation times τ and amplitudes A) obtained by stopped-flow measurements for mixing of equimolar amounts of eIF4E with 7-methyl-GpppG at concentration C for different ionic strengths corresponding to indicated concentrations of added KCl. The last column shows relative improvement of the fit with two relaxations over the fit with one relaxation, $\frac{\delta_s - \delta_d}{\delta_d}$.

Table A1 Added KCl 350 mM

C (μM)	Number of traces	Number of relaxation terms					$\frac{\delta_s - \delta_d}{\delta_d}$
		One	Two				
		$1/\tau$ (1/sec)	$1/\tau_1$ (1/sec)	A_1 (relative)	$1/\tau_2$ (1/sec)	A_2 (relative)	
0.2	600	51.5 ± 2.5	70.4 ± 19	0.78 ± 0.17	23.4 ± 7.5	0.22 ± 0.17	0.01
0.3	640	55.7 ± 1.5	83.9 ± 13.9	0.71 ± 0.15	30.0 ± 8.0	0.29 ± 0.15	0.02
0.4	168	51.3 ± 1.0	75.4 ± 8.9	0.56 ± 0.04	36.8 ± 6.1	0.44 ± 0.04	0.01
0.4	440	58.5 ± 1.3	72.5 ± 9.6	0.60 ± 0.20	46.6 ± 8.1	0.40 ± 0.20	0.01
0.5	320	64.3 ± 1.1	82.1 ± 15.	0.65 ± 0.30	46.3 ± 15.5	0.35 ± 0.30	0.01
0.6	168	68.7 ± 0.9	93.0 ± 6.9	0.65 ± 0.07	46.3 ± 5.3	0.35 ± 0.07	0.02
0.8	210	71.0 ± 0.6	91.6 ± 4.6	0.63 ± 0.07	50.1 ± 3.7	0.37 ± 0.07	0.02
1.0	126	75.0 ± 0.9	101. ± 7.2	0.61 ± 0.07	54.4 ± 5.6	0.39 ± 0.07	0.01
1.1	112	79.5 ± 1.0	126. ± 7.5	0.45 ± 0.03	62.2 ± 2.1	0.55 ± 0.03	0.02
1.3	168	83.3 ± 0.7	136. ± 9.5	0.45 ± 0.05	64.4 ± 3.5	0.55 ± 0.05	0.05
1.5	168	90.1 ± 0.8	146. ± 8.6	0.48 ± 0.05	67.8 ± 3.7	0.52 ± 0.05	0.07
1.7	224	98.1 ± 0.6	169. ± 8.9	0.45 ± 0.04	75.1 ± 2.8	0.55 ± 0.04	0.14
1.8	168	103. ± 0.7	155. ± 9.2	0.62 ± 0.07	66.8 ± 6.1	0.38 ± 0.07	0.22
1.8	168	99.8 ± 0.7	191. ± 21.	0.43 ± 0.07	74.7 ± 3.6	0.57 ± 0.07	0.24
2.0	168	109. ± 0.7	174. ± 10.	0.53 ± 0.05	79.3 ± 6.2	0.47 ± 0.05	0.17
2.0	168	105. ± 0.7	188. ± 8.9	0.50 ± 0.03	75.2 ± 3.2	0.50 ± 0.03	0.24
2.2	224	118. ± 0.7	205. ± 12.	0.54 ± 0.03	79.8 ± 3.5	0.46 ± 0.03	0.49
2.3	168	112. ± 0.7	216. ± 15.	0.48 ± 0.03	80.7 ± 3.1	0.52 ± 0.03	0.44
2.6	168	121. ± 0.7	196. ± 12.	0.54 ± 0.07	86.5 ± 6.5	0.46 ± 0.07	0.23
2.9	168	145. ± 0.8	232. ± 8.8	0.63 ± 0.04	91.0 ± 3.9	0.37 ± 0.04	0.75
3.4	168	143. ± 0.8	221. ± 6.7	0.69 ± 0.02	80.3 ± 3.4	0.31 ± 0.02	0.85
3.7	126	154. ± 0.8	246. ± 9.1	0.56 ± 0.03	112. ± 6.0	0.44 ± 0.03	0.28
4.1	126	165. ± 1.1	235. ± 5.8	0.80 ± 0.02	71.4 ± 3.9	0.20 ± 0.02	0.84

Table A2 Added KCl 150 mM

C (μM)	Number of traces	Number of relaxation terms					$\frac{\delta_s - \delta_d}{\delta_d}$
		One	Two				
		$1/\tau$ (1/sec)	$1/\tau_1$ (1/sec)	A_1 (relative)	$1/\tau_2$ (1/sec)	A_2 (relative)	
0.1	800	38.3 ± 1.0	47.6 ± 9.4	0.72 ± 0.31	27.0 ± 14.3	0.28 ± 0.31	0.00
0.2	660	48.8 ± 0.7	60.7 ± 6.6	0.75 ± 0.15	30.6 ± 7.6	0.25 ± 0.15	0.02
0.2	680	47.8 ± 0.7	49.5 ± 1.4	0.99 ± 0.03	17.0 ± 7.5	0.01 ± 0.03	0.01
0.3	560	58.0 ± 0.6	70.1 ± 3.5	0.75 ± 0.09	37.7 ± 5.0	0.25 ± 0.09	0.02
0.4	372	62.5 ± 0.7	118. ± 13.	0.31 ± 0.08	51.3 ± 2.5	0.69 ± 0.08	0.04
0.5	400	72.1 ± 0.5	103. ± 12.	0.42 ± 0.25	60.5 ± 11.	0.58 ± 0.25	0.03
0.6	600	83.8 ± 0.5	110. ± 3.6	0.69 ± 0.05	54.6 ± 3.5	0.31 ± 0.05	0.11
0.7	300	85.8 ± 0.7	137. ± 6.8	0.55 ± 0.06	60.3 ± 3.2	0.45 ± 0.06	0.13
0.8	480	95.7 ± 0.6	152. ± 7.8	0.50 ± 0.07	71.4 ± 5.0	0.50 ± 0.07	0.21
0.8	210	94.8 ± 0.8	201. ± 22.	0.43 ± 0.06	70.7 ± 3.4	0.57 ± 0.06	0.22
1.0	320	105. ± 0.7	176. ± 9.4	0.51 ± 0.07	77.5 ± 5.3	0.49 ± 0.07	0.21
1.1	224	116. ± 1.0	196. ± 8.0	0.57 ± 0.04	79.7 ± 4.4	0.43 ± 0.04	0.30
1.2	280	126. ± 0.8	177. ± 8.2	0.71 ± 0.06	75.1 ± 4.3	0.29 ± 0.06	0.24
1.3	320	126. ± 0.7	215. ± 11.	0.50 ± 0.06	94.4 ± 4.3	0.50 ± 0.06	0.30
1.3	168	130. ± 1.0	216. ± 11.	0.61 ± 0.04	81.9 ± 4.3	0.39 ± 0.04	0.43
1.5	168	143. ± 1.0	223. ± 9.0	0.65 ± 0.04	89.6 ± 5.6	0.35 ± 0.04	0.28
1.5	168	144. ± 1.1	217. ± 9.0	0.71 ± 0.04	81.9 ± 5.6	0.29 ± 0.04	0.34
1.7	224	152. ± 1.0	245. ± 8.0	0.68 ± 0.03	84.7 ± 3.8	0.32 ± 0.03	0.79
1.8	168	147. ± 1.0	238. ± 14.	0.61 ± 0.06	93.1 ± 6.0	0.39 ± 0.06	0.37
1.8	168	158. ± 1.0	243. ± 10.	0.63 ± 0.04	105. ± 7.0	0.37 ± 0.04	0.24
1.8	224	153. ± 1.0	253. ± 10.	0.63 ± 0.03	94.5 ± 4.4	0.37 ± 0.03	0.60
2.0	168	164. ± 1.0	256. ± 14.	0.64 ± 0.05	103. ± 5.9	0.36 ± 0.05	0.40
2.0	168	171. ± 1.1	282. ± 14.	0.65 ± 0.04	103. ± 5.4	0.35 ± 0.04	0.48
2.2	168	180. ± 1.1	281. ± 9.0	0.73 ± 0.03	93.6 ± 4.2	0.27 ± 0.03	0.94
2.6	168	193. ± 1.3	278. ± 7.2	0.81 ± 0.02	82.2 ± 4.3	0.19 ± 0.02	0.87
3.0	168	212. ± 1.4	305. ± 7.5	0.80 ± 0.02	97.2 ± 4.9	0.20 ± 0.02	0.86
3.4	168	242. ± 1.5	327. ± 6.4	0.85 ± 0.02	95.6 ± 5.0	0.15 ± 0.02	0.96
3.4	168	226. ± 1.4	329. ± 9.8	0.78 ± 0.03	113. ± 5.9	0.22 ± 0.03	0.74
4.1	126	254. ± 1.7	375. ± 11.	0.80 ± 0.02	121. ± 6.0	0.20 ± 0.02	0.71
4.1	126	251. ± 2.8	375. ± 16.	0.81 ± 0.03	118. ± 10.	0.19 ± 0.03	0.68

Table A3 Added KCl 50 mM

C (μM)	Number of traces	Number of relaxation terms					$\frac{\delta_s - \delta_d}{\delta_d}$
		One	Two				
		$1/\tau$ (1/sec)	$1/\tau_1$ (1/sec)	A_1 (relative)	$1/\tau_2$ (1/sec)	A_2 (relative)	
0.05	1440	32.8 ± 0.6	34.9 ± 0.7	0.97 ± 0.01	4.0 ± 1.6	0.03 ± 0.01	0.024
0.1	880	45.6 ± 0.5	57.5 ± 4.3	0.79 ± 0.09	24.9 ± 4.8	0.21 ± 0.09	0.04
0.1	600	50.3 ± 1.2	58.5 ± 5.1	0.93 ± 0.05	11.9 ± 3.7	0.07 ± 0.05	0.03
0.2	1080	65.0 ± 0.5	95.3 ± 4.8	0.61 ± 0.06	43.6 ± 6.8	0.39 ± 0.06	0.11
0.2	900	66.4 ± 0.5	83.4 ± 4.8	0.72 ± 0.10	44.8 ± 6.8	0.28 ± 0.10	0.06
0.3	440	82.1 ± 0.6	120. ± 6.0	0.65 ± 0.05	51.8 ± 4.0	0.35 ± 0.05	0.18
0.3	440	83.0 ± 1.6	151. ± 8.6	0.45 ± 0.06	64.0 ± 4.0	0.55 ± 0.06	0.18
0.3	448	97.9 ± 1.5	121. ± 6.3	0.89 ± 0.04	28.8 ± 7.1	0.11 ± 0.04	0.08
0.4	294	133. ± 1.7	159. ± 11.	0.83 ± 0.08	74.8 ± 18.	0.17 ± 0.08	0.02
0.5	252	146. ± 1.7	163. ± 8.3	0.95 ± 0.05	42.8 ± 14.	0.05 ± 0.05	0.04
0.5	448	135. ± 1.0	160. ± 6.9	0.88 ± 0.05	60.5 ± 10.9	0.12 ± 0.05	0.09
0.6	720	129. ± 0.7	204. ± 11.	0.61 ± 0.05	84.3 ± 4.7	0.39 ± 0.05	0.42
0.6	300	167. ± 1.6	194. ± 6.8	0.94 ± 0.03	45.6 ± 9.3	0.06 ± 0.03	0.12
0.6	224	181. ± 2.4	230. ± 17.	0.63 ± 0.11	141. ± 17.	0.37 ± 0.11	0.00
0.6	280	151. ± 1.9	235. ± 18.	0.70 ± 0.06	85.2 ± 9.9	0.30 ± 0.06	0.09
0.7	280	180. ± 1.6	252. ± 14.	0.73 ± 0.06	106. ± 12.	0.27 ± 0.06	0.10
0.8	280	184. ± 1.4	258. ± 10.	0.77 ± 0.04	95.1 ± 7.7	0.23 ± 0.04	0.25
0.9	480	175. ± 1.1	226. ± 11.	0.75 ± 0.06	95.8 ± 9.1	0.25 ± 0.06	0.18
0.9	224	205. ± 1.8	303. ± 14.	0.66 ± 0.05	139. ± 10.	0.34 ± 0.05	0.08
1.0	440	182. ± 1.1	281. ± 12.	0.68 ± 0.04	109. ± 6.2	0.32 ± 0.04	0.49
1.0	320	203. ± 1.5	288. ± 9.9	0.78 ± 0.03	106. ± 7.3	0.22 ± 0.03	0.29
1.1	224	245. ± 1.9	311. ± 13.	0.85 ± 0.04	111. ± 14.	0.15 ± 0.04	0.17
1.2	340	206. ± 1.3	316. ± 12.	0.71 ± 0.03	116. ± 6.5	0.29 ± 0.03	0.55
1.3	360	228. ± 1.4	334. ± 11.	0.77 ± 0.03	119. ± 6.6	0.23 ± 0.03	0.62
1.4	280	302. ± 2.5	373. ± 11.	0.91 ± 0.02	106. ± 13.	0.09 ± 0.02	0.23
1.5	224	281. ± 1.8	372. ± 18.	0.76 ± 0.06	166. ± 19.	0.24 ± 0.06	0.15
1.6	360	249. ± 2.2	353. ± 6.1	0.89 ± 0.01	71.7 ± 3.4	0.11 ± 0.01	0.49
1.8	340	285. ± 1.8	407. ± 14.	0.80 ± 0.03	147. ± 10.	0.20 ± 0.03	0.49
1.8	224	337. ± 2.3	420. ± 15.	0.79 ± 0.05	202. ± 15.	0.21 ± 0.05	0.08

References

Antosiewicz J (1995) Computation of the dipole moments of proteins. Biophys J 69: 1344–1354

Antosiewicz J, McCammon JA (1995) Electrostatic and hydrodynamic orientational steering effects in enzyme-substrate association. Biophys J 69: 57–65

Antosiewicz J, Porschke D (1989) Volume correction for bead model simulations of rotational friction coefficient of macromolecules. J Phys Chem 93: 5301–5305

Antosiewicz J, Gilson MK, Lee IH, McCammon JA (1995) Acetylcholinesterase: diffusional encounter rate constants for dumbbell models of a ligand. Biophys J 68: 62–68

Antosiewicz J, Briggs JM, Elcock AE, Gilson MK, McCammon JA (1996) Computing the ionization states of proteins with a detailed charge model. J Comput Chem 17: 1633–1644

Bernasconi CF (1976) Relaxation kinetics. Academic Press, New York

Bernstein FC, Koettzle TF, Williams GJB, Meyer EF, Brice MD, Rodgers JR, Kennard O, Shimanouchi T, Tasumi MJ (1977) The protein data bank: a computer-based archival file for molecular structures. J Mol Biol 123: 557–594

Briggs JM, Antosiewicz J (1999) Simulation of p{H}-dependent properties of proteins using mesoscopic models. Rev Comput Chem 13: 249–311

Brooks BR, Bruccoleri RE, Olafson BD, States DJ, Swaminathan S, Karplus M (1983) CHARMM: a program for macromolecular energy, minimization, and dynamics calculations. J Comput Chem 4: 187–217

Brunger AT, Karplus M (1988) Polar hydrogen positions in proteins: empirical energy placement and neutron diffraction comparison. Proteins Struct Funct Genet 4: 148–156

Cai A, Jankowska-Anyszka M, Centers A, Chlebicka L, Stepinski J, Stolarski R, Darżynkiewicz E, Rhoads RE (1999) Quantitative assessment of mRNA cap analogs as inhibitors of in vitro translation. Biochemistry 38: 8538–8547

Carberry SE, Rhoads RE, Goss DJ (1989) A spectroscopic study of binding of m7GTP and m7GpppG to human protein synthesis initiation factor 4E. Biochemistry 28: 8078–8082

Darżynkiewicz E, Stępiński J, Tahara SM, Stolarski R, Ekiel I, Haber D, Neuvonen K, Lehikoinen P, Labadi I, Lönnberg H (1990) Synthesis, conformation and hydrolytic stability of P^1,P^3-dinucleoside triphosphates related to mRNA 5′-cap, and comparative kinetic studies of their nucleoside and nucleoside monophosphate analogs. Nucleosides Nucleotides 9: 599–618

Davis ME, Madura JD, Luty BA, McCammon JA (1991) Electrostatics and diffusion of molecules in solution: simulations with the University of Houston Brownian dynamics program. Comput Phys Commun 62: 187–197

Deutch JM, Felderhof BU (1973) Hydrodynamic effect in diffusion-controlled reaction. J Chem Phys 59: 1669–1671

Eigen M, De Maeyer L (1974) Theoretical principles of relaxation spectroscopy. In: Hammes GG (ed) Investigation of rates and mechanisms of reactions. Wiley, New York, pp 79–172

Ermak DL, McCammon JA (1978) Brownian dynamics with hydrodynamic interactions. J Chem Phys 69: 1352–1360

Friedman HL (1966) A hydrodynamic effect in the rates of diffusion-controlled reactions. J Phys Chem 70: 3931–3933

Garcia de la Torre J, Bloomfield VA (1981) Hydrodynamic properties of complex, rigid, biological macromolecules: theory and applications. Q Rev Biophys 14: 81–139

Gilson MK, Sharp KA, Honig BH (1988) Calculating the electrostatic potential of molecules in solution: method and error assessment. J Comput Chem 9: 327–335

Kramers HA (1940) Brownian motion in a field of force and the diffusion model of chemical reactions. Physica 7: 284–304

Lakowicz JR (1983) Principles of fluorescence spectroscopy. Plenum Press, New York

Luty BA, El Amarani S, McCammon JA (1993) Simulation of the bimolecular reaction between superoxide and superoxide dismutase: synthesis of the encounter and reaction steps. J Am Chem Soc 115: 11874–11877

Madura JD, Briggs JM, Wade RC, Davis ME, Luty BA, Ilin A, Antosiewicz J, Gilson MK, Bagheri B, Scott LR, McCammon JA (1995) Electrostatics and disffusion of molecules in solution: simulations with the University of Houston Brownian dynamics program. Comput Phys Commun 91: 57–95

Marcotrigiano J, Gingras A, Sonenberg N, Burley SK (1997) Cocrystal structure of the messenger RNA 5′ cap-binding protein (eIF4E) bound to 7-methyl-GDP. Cell 89: 951–961

Matsuo H, Li H, McGuire AM, Fletcher CM, Gingras A, Sonenberg N, Wagner G (1997) Structure of translation factor eIF4E bound to m^7GDP and interaction with 4E-binding protein. Nat Struct Biol 4: 717–724

Merrick WC, Hershey JWB (1996) The pathway and mechanism of eukaryotic protein synthesis. In: Hershey J, Mathews MB, Sonenberg N (eds) Translation control. Cold Spring Harbor Laboratory Press, New York, pp 31–69

Molecular Simulations (1992a) Polar hydrogen parameter set for CHARMm version 22 (polar hydrogens only). Molecular Simulations, Waltham, Mass

Molecular Simulations (1992b) InsightII. Molecular Simulations, San Diego, Calif

Northrup SH, Allison SA, McCammon JA (1984) Brownian dynamics simulation of diffusion-influence bimolecular reactions. J Chem Phys 80: 1517–1524

Richards FM (1977) Areas, volumes, packing and protein structure. Annu Rev Biophys Bioeng 6: 151–176

Sha M, Wang Y, Xiang T, van Heerdens A, Browning KS, Goss DJ (1995) Interaction of wheat germ protein synthesis initiation factor eIF-(iso)4F and its subunits p28 and p86 with m^7GTP and mRNA analogues. J Biol Chem 270: 29904–29909

Shatkin AJ (1976) Capping of eukaryotic mRNAs. Cell 9: 645–653

Smoluchowski M von (1917) Versuch einer mathematischen theorie der koagulationskinetik kolloider losungen. Z Phys Chem 92: 129–168

Sonenberg N (1996) mRNA 5′ cap-binding protein eIF4E and control of cell growth. In: Hershey J, Mathews MB, Sonenber N (eds) Translation control. Cold Spring Harbor Laboratory Press, New York, pp 245–269

Stępiński J, Bretner M, Jankowska M, Felczak K, Stolarski R, Wieczorek Z, Cai A, Rhoads RE, Haber D, Darżynkiewicz E (1995) Synthesis and properties of P^1,P^2-, P^1,P^3-, and P^1,P^4-dinucleoside di-, tri- and tetraphosphate mRNA 5′-cap analogues. Nucleosides Nucleotides 14: 717–721

Wade RC, Davis ME, Luty BA, Madura JD, McCammon JA (1993) Gating of the active site of triose phosphate isomerase: Brownian dynamics simulations of flexible peptide loops in the enzyme. Biophys J 64: 9–15

Warwicker J, Watson HC (1982) Calculation of the electric potential in the active site cleft due to α-helix dipoles. J Mol Biol 157: 671–679

Wieczorek Z, Stępiński J, Jankowska M, Lönnberg H (1995) Fluorescence and absorption spectroscopic properties of RNA 5′-cap analogues derived from 7-methyl-, N^2,7-dimethyl- and N^2,N^2,7-trimethyl-guanosines. J Photochem Photobiol 28: 57–63

Wieczorek Z, Zdanowski K, Chlebicka L, Stępiński J, Jankowska M, Kierdaszuk B, Temeriusz A, Darżynkiewicz E, Stolarski R (1997) Fluorescence and NMR studies of intramolecular stacking mRNA cap-analogues. Biochim Biophys Acta 1354: 145–152

Wieczorek Z, Darżynkiewicz E, Lonnberg H (1998) A fluorescence study on the binding of mRNA 5′-cap-analogs to human translation initiation factor eIF4E: a critical evaluation of the sources of error. J Photochem Photobiol B 43: 158–163

Yamakawa H (1970) Transport properties of polymer chains in dilute solutions. Hydrodynamic interactions. Chem Phys 53: 436–443